Nitrogen-Doped Partially Reduced Graphene Oxide Rewritable Nonvolatile Memory

Sohyeon Seo,[†] Yeoheung Yoon,[‡] Junghyun Lee,[†] Younghun Park,[†] and Hyoyoung Lee[†,‡,*]

[†]National Creative Research Initiative, Center for Smart Molecular Memory, Department of Chemistry, Sungkyunkwan University, 300 Cheoncheon-dong, Jangan-gu, Suwon, Gyeonggi-do 440-746, Korea, and [‡]Department of Energy Science, Sungkyunkwan University, 300 Cheoncheon-dong, Jangan-gu, Suwon, Gyeonggi-do 440-746, Korea

ABSTRACT

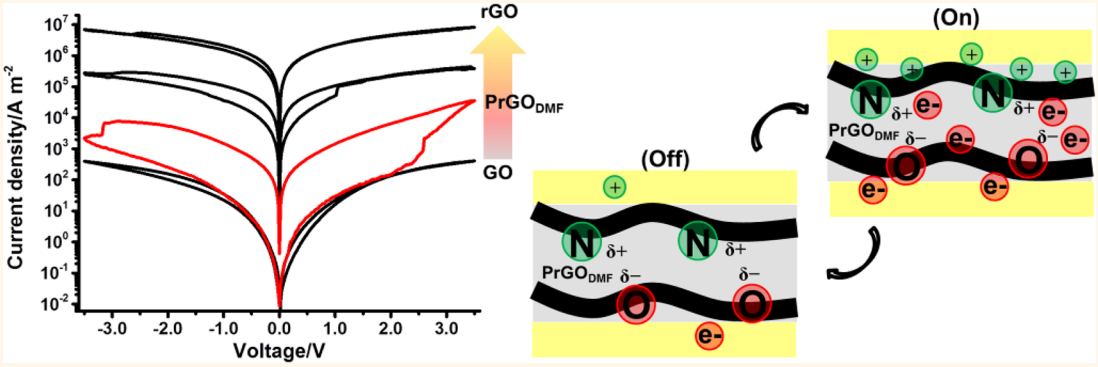

As memory materials, two-dimensional (2D) carbon materials such as graphene oxide (GO)-based materials have attracted attention due to a variety of advantageous attributes, including their solution-processability and their potential for highly scalable device fabrication for transistor-based memory and cross-bar memory arrays. In spite of this, the use of GO-based materials has been limited, primarily due to uncontrollable oxygen functional groups. To induce the stable memory effect by ionic charges of a negatively charged carboxylic acid group of partially reduced graphene oxide (PrGO), a positively charged pyridinium N that served as a counterion to the negatively charged carboxylic acid was carefully introduced on the PrGO framework. Partially reduced N-doped graphene oxide (PrGO$_{DMF}$) in dimethylformamide (DMF) behaved as a semiconducting nonvolatile memory material. Its optical energy band gap was 1.7−2.1 eV and contained a sp^2 C═C framework with 45−50% oxygen-functionalized carbon density and 3% doped nitrogen atoms. In particular, rewritable nonvolatile memory characteristics were dependent on the proportion of pyridinum N, and as the proportion of pyridinium N atom decreased, the PrGO$_{DMF}$ film lost memory behavior. Polarization of charged PrGO$_{DMF}$ containing pyridinium N and carboxylic acid under an electric field produced N-doped PrGO$_{DMF}$ memory effects that followed voltage-driven rewrite-read-erase-read processes.

KEYWORDS: nonvolatile memory · partially reduced graphene oxide · nitrogen doping · polarization · optical band gap

Organic rewritable nonvolatile memory that shows repeatable switching between different conducting states would be a highly versatile memory usable in numerous applications. Since the active layer could be highly scalable, organic or hybrid organic−inorganic semiconductors have been of interest due to their compatibility with low-cost, high-throughput processing techniques.[1] For example, small organic molecules, oligomers, and polymers which have π-conjugated molecular systems or electroactive systems have been used as engineered materials that can be fabricated by simple solution-deposition or vapor-deposition processing into robust nonvolatile memory electronic devices.[2] Because of process advantages such as chemical functionalization or hybrid composites, π-conjugated carbon materials such as pentacene,[3] fullerene,[4] carbon nanotubes,[5] and graphene oxide (GO)[6,7] have attracted considerable attention in memory applications. In particular, GO has shown promising nonvolatile memory characteristics. Nonvolatile memory devices with GO as the active material and Al−Al[8] and Al−ITO as the top and bottom electrodes showed

* Address correspondence to hyoyoung@skku.edu.

Received for review February 4, 2013 and accepted March 22, 2013.

Published online March 23, 2013
10.1021/nn400588u

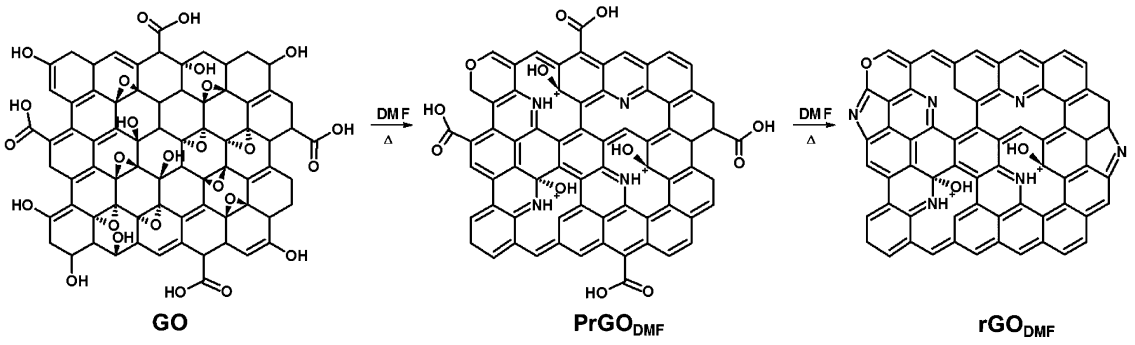

Scheme 1. Schematic solvothermal reduction process of graphene oxide in DMF for the creation of N-doped partially reduced graphene oxide nonvolatile memory materials

electrically rewritable characteristics in a cross-bar memory cell, but devices using Au−ITO[9] and graphene−graphene were not rewritable.[10] Thus, an origin of the rewritable memory characteristics does not from GO, but rather from the Al metal particles serving as the memory material. The electrical diffusion of oxygen atoms or the electrochemical reaction of oxygen-containing groups could result in memory behaviors.[8−11] The resistivity switching of GO or partially reduced GOs can be reversible in electrochemically active metal contacts (*e.g.*, Al)[8] and irreversible in electrochemically inactive metal contacts (*e.g.*, Au)[9] or graphene contacts.[10] Thus, until now, there is no report on that GO by itself can be used as a rewritable memory material.

It is suggested that an existence of a negatively charged carboxylic acid and a positively charged cation functional group in nitrogen-doped partially reduced GO (PrGO) may produce an easy polarization that leads to be used as a memory material under an electric field. It is also expected that an association between charged functional groups may generate a charge transport path to increase the operational ON/OFF ratio of rewritable memory devices for the voltage-induced polarized film. For example, the N-doped PrGO containing pyridinium N as a counterionic functional group to the negatively charged carboxylic acid (*e.g.*, $H^{\delta+}$N-PrGO−$COO^{\delta-}$/$H^{\delta+}$N-PrGO−$COO^{\delta-}$ or H^{+}N-PrGO−COO^{-}/H^{+}N-PrGO−COO^{-}) should be one of potential materials. In addition, the reversible resistive memory effects for the diffusion of oxygen on the graphene plane can be taken into account. The charge carrier density on the graphene plane should determine the memory behavior of GO in the devices, which should be dependent on the degree of oxidation or reduction. Even though the role of the oxygen groups in GO is unclear, it is clear that the binding between the oxygen-containing functional groups of GO and the charges induced by the electrode materials strongly influence the nonvolatile memory characteristics. Thus, one of the important challenges in GO-based rewritable nonvolatile memory devices is facile control of the semiconducting property of GO at different oxygen density states (or charging states). Therefore, the control of the oxygen functional groups associated with the semiconducting characteristics of PrGO and the understanding of the specific polarization through the dipole−dipole or hydrogen-bonding states of the oxygen-functional groups under an electric field and the rewritable nonvolatile memory behavior are crucial. Semiconducting GO or graphene possessing different energy band gaps has been synthesized by the reduction of GO. The energy band gaps of chemically reduced GO and thermally reduced GO can be controlled in the range of 2.2 to 0.5 eV.[12]

Herein, we present novel GO-based rewritable nonvolatile memory materials containing nitrogen atoms with controlled energy band gaps (Scheme 1). Since GO sheets in thin films are stacked, oxygen functional groups between neighboring sheets could form hydrogen bonds due to intercalated water molecules or the presence of solvent.[13] During the reduction of GO, the intercalated molecules can aid in the generation or loss of bonds between the GO sheets. To precisely control the energy band gap of GO to produce a suitable memory material, strong reducing reagents such as hydrazine and hydroiodide should be avoided. Thus, dimethylformamide (DMF), a polar aprotic solvent, was chosen, since it is a good solvent for GO/PrGO and a mild reducing agent at elevated temperatures and can also serve as a nitrogen source.[14,15] During the thermal reduction of GO in DMF, nitrogen doping (the formation of C−N bonds), which forms the active sites for the memory activity of PrGO, could occur. Because of the mild reduction capability of DMF, it is expected that pyridinic N-doped PrGO would be the predominant species synthesized instead of pyrrolic N-doped PrGO, which is produced by partially charged PrGO with pyridinium N and has an open energy band gap. It is believed that the association (including hydrogen-bonding interactions) between charged pyridinium N and charged carboxylic oxygen at the interlayers of N-doped PrGO sheets could induce the polarization of PrGO films under an electric field that leads to the voltage-driven conductance switching between On and OFF states in a memory device.

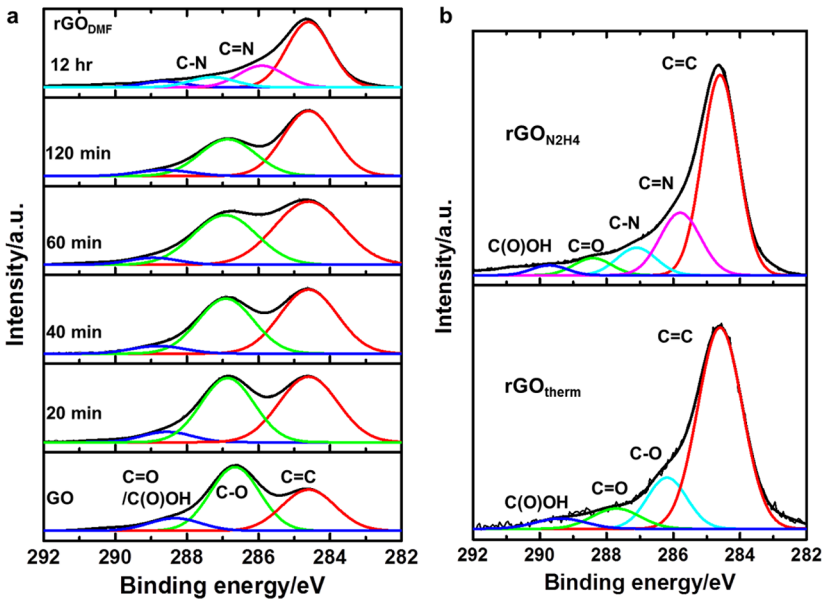

Figure 1. XPS spectra of C1s of (a) GO, PrGO$_{DMF}$, and rGO$_{DMF}$, (b) rGO$_{N2H4}$ and rGO$_{therm}$ (at 300 °C).

Reported herein are the rewritable nonvolatile memory characteristics of chemically synthesized semiconducting N-doped PrGOs with different band gap values. Regarding the oxygen-functionalized carbon density, rewritable nonvolatile memory behaviors were found to be significant for an oxygen-functionalized carbon density of 45−50%. On the other hand, the current hysteresis of the current−voltage characteristics is negligible when fully reduced GO has a low oxygen-functionalized carbon density and when highly oxidized GO has a high oxygen-functionalized carbon density. As a whole, our proposal suggests that a suitable density of oxygen functional groups is required to form $H^{\delta+}$N-PrGO−$COO^{\delta-}$/$H^{\delta+}$N-PrGO−$COO^{\delta-}$ between the interlayers of pyridinium N-activated N-doped PrGO$_{DMF}$ sheets, and that a charge-controlled layer that allows for the control of the characteristics of polarization-induced rewritable nonvolatile memory could be formed.

RESULTS AND DISCUSSION

Solvothermally reduced GOs with DMF (PrGO$_{DMF}$ and rGO$_{DMF}$) and chemically reduced GO with hydrazine (*i.e.*, rGO$_{N2H4}$) were examined with X-ray photoelectron spectroscopy (XPS) to characterize chemical functionalities related to sp^2- or sp^3-carbon atoms. As shown in Figure 1, the deconvoluted C1s spectra of GO were assigned to the sp^2 carbon−carbon (C═C at 254.6 eV) peak and the sp^3 carbon−oxygen peaks (*e.g.*, the oxygen-containing groups such as hydroxyl/ether/epoxy (C−O at 286.6 eV) and carbonyl/carboxyl (C═O/C(O)OH at 288.6 eV)). As shown in Figure 1, the sp^2 carbon−carbon peak gradually increased, whereas the sp^3 carbon−oxygen peaks gradually decreased as the reaction time increased. Eventually, after a 12-h reaction (rGO$_{DMF}$), the C−O and the C═O peaks significantly decreased and new peaks representing C═N at 285.9 eV and C−N at 287.3 eV were observed,[16] which were nearly identical with those of rGO$_{N2H4}$ (Figure 1) except for the existence of a C═O peak at 288.4 eV replacing the C(O)OH peak at 288.9 eV.[17] In contrast to rGO$_{DMF}$ and rGO$_{N2H4}$, GO thermally reduced at 300 °C (rGO$_{therm}$) did not show noticeable C−N peaks, indicating that DMF and N_2H_4 supplied N atoms for the binding formation of C−N. The changes in the peak intensity or area of the C1s spectra suggest changes in the oxygen coverage of carbon atoms or the oxygen configurations in the solvothermal reaction. For a detailed quantitative analysis of the degree of oxygen atoms bounded to carbon atoms, the C1s XPS spectra of GO, PrGO$_{DMF}$, rGO$_{DMF}$, and rGO$_{N2H4}$ were used to determine the oxygen coverage to carbon atoms that was given by the area ratio of the deconvoluted carbon−oxygen peaks over the convoluted C1s peak (Table S1, Supporting Information). Consequently, the oxygen-functionalized carbon density was decreased as the oxygen-containing functional groups were eliminated by the solvothermal reduction. The defunctionalization of the carbon atoms led to a decrease in the oxygen-functionalized carbon density, which gradually decreased from 70.6% (GO) to 41.4% (120 min PrGO$_{DMF}$) and to 36.5% (rGO$_{DMF}$). As shown in Figure 1, rGO$_{N2H4}$ has an oxygen-functionalized carbon density of 34.3%, which was similar to that of rGO$_{DMF}$. The XPS spectra confirmed that DMF acted as a mild reducing agent for GO. Furthermore, in the same manner, GO dispersed in pure DI water was much less reduced than in DMF (Figure S1, Supporting Information).

In addition to the mild reduction of GO, DMF acted as a source of N atoms for N-doped PrGO$_{DMF}$, which was also confirmed by the XPS spectra of PrGO$_{DMF}$ and rGO$_{DMF}$ showing significant N1s peaks (Figures 2a

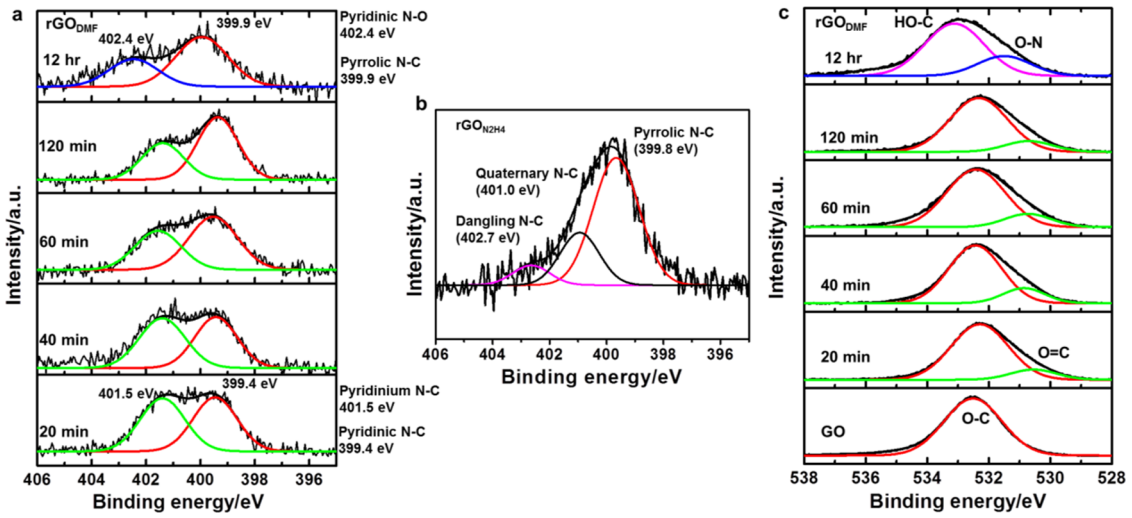

Figure 2. (a and b) XPS spectra of N1s of (a) $PrGO_{DMF}$ and rGO_{DMF}, (b) rGO_{N2H4}. (c) XPS spectra of O1s of GO, $PrGO_{DMF}$, and rGO_{DMF}.

and 2b), corresponding to >3% of the N atoms. The deconvoluted N1s spectra of $PrGO_{DMF}$ were assigned to the pyridinic N−C peak at 399.4 eV and the pyridinium N−C peak at 401.5 eV.[18,19] As the reaction time increased, the pyridinium N−C peak gradually decreased, whereas the pyridinic N−C peak gradually increased. Eventually, after a 12 h-reaction (rGO_{DMF}), the pyridinium N−C peak vanished and new peaks of pyridinic N−O at 402.4 eV and pyrrolidic N−C at 399.9 eV were observed.[20] Unlike the N1s peak of rGO_{N2H4},[21] a quaternary N−C peak at 401.0 eV and a dangling N−C peak at 402.7 eV were not observed. The N1s XPS spectra indicated that during the solvothermal reduction with DMF, the association between the oxygen groups of GO and the N atoms of DMF could be involved in new N−O bonds *via* an intermediate form of the pyridinium $^{+}$N−C. The O1s XPS spectra (Figure 2c) also revealed the new N−O bond at 531.5 eV for rGO_{DMF} after a 12 h-reaction. Therefore, the N-mediated reduction of GO could occur along with the formation of a pyridinium N intermediate and the production of N-doped rGO_{DMF}.

Structural changes due to the reduction of GO were characterized by Raman spectra (Figure 3a). First-order G- and D-bands originating from the vibrations of sp^2 carbon appeared at 1597−1609 cm^{-1} (from GO to rGO_{DMF}) and 1350−1360 cm^{-1} (from GO to rGO_{DMF}), respectively. The intensity ratio of the D-band to the G-band increased as GO sheets ($I_D/I_G < 0.8$) converted to $PrGO_{DMF}$ sheets ($0.8 < I_D/I_G < 0.9$) and to 12 h rGO_{DMF} ($I_D/I_G > 0.9$). An increase in the I_D/I_G ratio indicated an increase in the defect density correlating with the defunctionalization of the oxygen functional groups. In particular, the G-bands shifted considerably with regards to reaction time. Electron-doping effects due to the insertion or bond formation of N atoms to the sp^2-carbon framework led to a red-shift in the G-bands of $PrGO_{DMF}$ (20 min, 40 min, and 60 min) and rGO_{DMF}. At 120 min, the G-band of $PrGO_{DMF}$ was markedly blue-shifted (Figure 3b), which might be the result of a transition state between two different doping types of pyridinium- and pyridinic-N atoms in the sp^2-carbon framework. The catalytic activity of pyridinium N during the reduction of oxygen groups on the neighboring $PrGO_{DMF}$ sheets resulted in highly reduced $PrGO_{DMF}$ compared to $PrGO_{water}$ (Figure S1, Supporting Information), which can also be clearly observed by the formation of pyridinic N−O. Furthermore, the formation of N-doped $PrGO_{DMF}$ was also identified by Fourier transform infrared (FT-IR) spectroscopy (Figure 3c). In the IR spectrum of GO, the characteristic bands of C═O at 1730 cm^{-1}, C═C at 1620 cm^{-1}, and C−O at 1050 cm^{-1} could be identified. After the reduction of GO to $PrGO_{DMF}$, the C═O peak decreased relative to the C═C peak. The absorption in the 1200−1600 cm^{-1} range can be attributed to the N atoms bonded into the sp^2 carbon framework.[22] Thus, the new peak at 1550 cm^{-1} can be attributed to C−N in $PrGO_{DMF}$ and a peak at 1662 cm^{-1} in rGO_{N2H2} can be attributed to C═N,[21] whereas no peak associated with N atoms on rGO_{therm} was found (Figure 3d).

As the N-doping and reduction of GO proceeded in the DMF solution, the restoration of the π-conjugated structures induced the gradual red-shifting of the peak at 230 nm (attributed to the $\pi-\pi^*$ transition of C═C bond) in the UV−vis spectra of GO and $PrGO_{DMF}$ powder (Figure S2, Supporting Information). The diffuse reflectance UV−vis spectra of the $PrGO_{DMF}$ powder were measured to obtain the band gap. This technique has generally been used for particles, including rGOs (or graphite oxide). The band gap energy was determined by the Kubulka-Munk method, defined as $F(R) = (1-R)^2/(2R)$, where R is reflectance and $F(R)$ is proportional to the extinction coefficient.[23,24] Figure 4a shows plots of the modified Kubulka-Munk function *versus* the band gap energies of $PrGO_{DMF}$, in

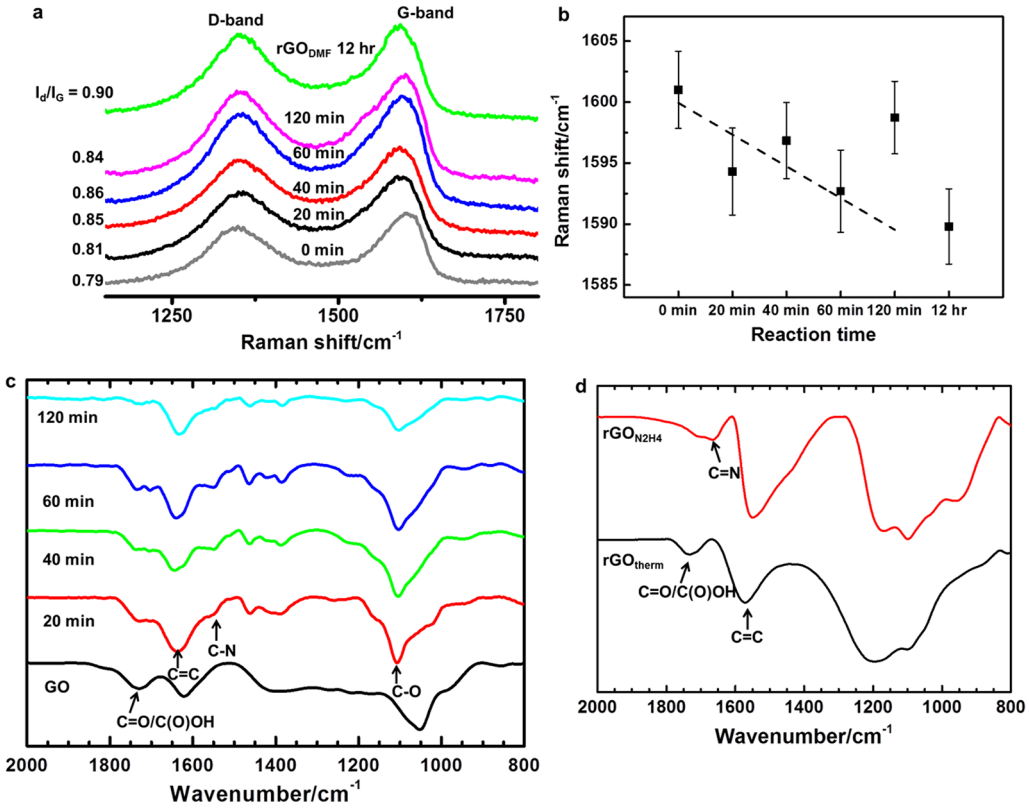

Figure 3. (a) Raman spectra of (a) GO, PrGO$_{DMF}$, and rGO$_{DMF}$. (b) Plots of G-bands for GO, PrGO$_{DMF}$, and rGO$_{DMF}$. The error bars indicate standard deviation. (c and d) FTIR spectra of (c) GO and PrGO$_{DMF}$, (d) rGO$_{N2H4}$ and rGO$_{therm}$ (at 300 °C).

which the modified Kubulka-Munk function is the $F(R)$ function in terms of $h\nu$, where h is Plank's constant and ν is the light frequency. The band gap energy decreased from 2.55 eV (GO) to 1.35 eV (120 min PrGO$_{DMF}$) as the reaction time increased. The band gap energy of GO significantly decreased by 50% during the 120 min of reduction to PrGO$_{DMF}$, which is presumably associated with a significant decrease (~30%) in the oxygen-functionalized carbon density and the C═O groups in particular, as shown in FT-IR spectra (Figure 3c). One of the noticeable phenomena in the plots of the modified Kubulka-Munk function was a significant decrease of the band gap energy after 120 min of reaction, which also appeared in the XPS, Raman, and FT-IR spectra with the same frequency.

To understand the change in the interlayer of PrGO$_{DMF}$ films with reaction time, X-ray diffraction (XRD) was used. Figure 4b shows the reduction time-dependent evolution of the peaks for the (002) facet of graphene. As the reduction reaction gradually proceeded, two types of the (002) peaks appeared and shifted to the right. Peak A at 2θ = ~10−12° gradually decreased over the 60 min reaction time and nearly merged into Peak B at 2θ = ~24.5° after 120 min. Interestingly, the position of Peak A of GO was observed at a higher degree (11.26°) than those of PrGO$_{DMF}$ at 20−40 min, indicating that the intercalations of certain molecules such as DMF can produce a larger interlayer distance in PrGO$_{DMF}$ at 20−40 min (8.816 and 8.037 Å), as compared with GO (7.852 Å). The interlayer distances of Peak B gradually decreased from 3.887, 3.811, and 3.789 Å for PrGO$_{DMF}$ at 20−60 min to 3.645 Å for 120 min PrGO$_{DMF}$ and to 3.559 Å for PrGO$_{DMF}$ at 12 h (Figure S3, Supporting Information). In particular, a drastic change in the XRD pattern of PrGO$_{DMF}$ is that Peak A faded to merge into Peak B in PrGO$_{DMF}$ at 120 min. It is reasonable to assume that the interlayer distance decreased as the reduction proceeded due to removal of intercalated water molecules and oxygen functional groups. Furthermore, the interlayer distance of rGO$_{therm}$ at 1000 °C was measured to be 3.43 Å (Figure S3, Supporting Information), which was very similar to that of graphite (~3.4 Å). Intercalated molecules, oxide groups, defects, or empty spaces between GO/PrGO/rGO sheets could produce interlayer distances larger than that of graphite.[25] In the same manner, doped nitrogen atoms from C−N bonds (chemical defects) could also have induced the increase in the interlayer distance. Considering the existence of pyridinic N−O in rGO$_{DMF}$ (in the XPS spectra) instead of pyridinium N, $H^{\delta+}$N-PrGO−$COO^{\delta-}$/$H^{\delta+}$N-PrGO−$COO^{\delta-}$ as an intermediate could be formed in the interlayers of PrGO$_{DMF}$. As the amount of doped nitrogen atoms was retained at 2.7−3.2% in PrGO$_{DMF}$, the pyridinium N in $H^{\delta+}$N-PrGO−$COO^{\delta-}$/$H^{\delta+}$N-PrGO−$COO^{\delta-}$ presumably was converted to pyridinic N−C or pyridinic N−O (as shown in

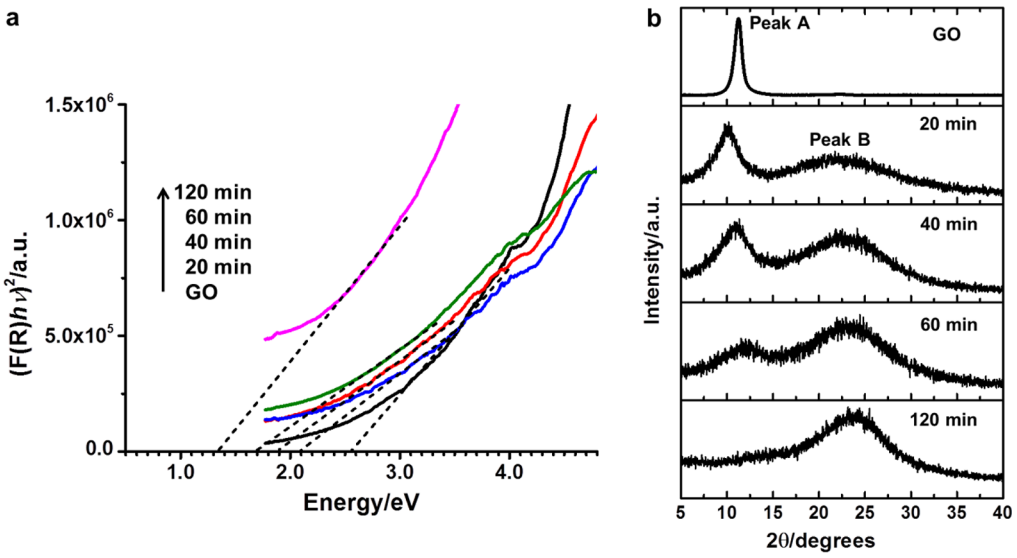

Figure 4. (a) Kubulka-Munk plots of UV−vis diffuse reflectance spectra *versus* the band gap energies for GO and $PrGO_{DMF}$. The extrapolated lines indicate the optical band gap energies of each sample. (b) XRD spectra of GO and $PrGO_{DMF}$.

Figure 2a). The significant loss of C═O (C(O)OH at 1730 cm^{-1}) in the FT-IR spectrum of $PrGO_{DMF}$ at 120 min suggests that the deformation of $H^{\delta+}$N-PrGO−$COO^{\delta-}$/$H^{\delta+}$N-PrGO−$COO^{\delta-}$ could occur. Therefore, the loss of Peak A in the XRD pattern of 120 min $PrGO_{DMF}$ was due to the loss of carboxyl groups in the interlayer.

Finally, the rewritable nonvolatile memory characteristics of $PrGO_{DMF}$ films with $H^{\delta+}$N-PrGO−$COO^{\delta-}$/$H^{\delta+}$N-PrGO−$COO^{\delta-}$ was demonstrated using a two-terminal crossbar memory device with the memory material sandwiched between the bottom and top electrodes (*e.g.*, metal/$PrGO_{DMF}$ thin film/metal) (Figure 5a). The thin film active layer on the ITO substrate was prepared by the spin coating of GO, $PrGO_{DMF}$, and rGO_{N2H4} (a control sample was used to represent fully reduced GO) dispersed in DMF solution. The electronic characteristics of each device were investigated in a low voltage range and a high voltage range. At a low voltage range from −0.5 V to +0.5 V, the electronic transport behaviors of the Au/thin film/ITO devices were examined. The current−voltage characteristics of the Au/$PrGO_{DMF}$/ITO devices showed sigmoidal curves, and in contrast to the linear *I*−*V* curve of Au/rGO_{N2H4}/ITO. At −0.5 V, the current value of 20 min $PrGO_{DMF}$ was increased by $\sim 10^5$ times over that of GO (see the *I*−*V* curve in inset), revealing a significant reduction effect accompanied by N-doping in DMF solution. Furthermore, operation performances of the Au/$PrGO_{DMF}$/ITO memory devices were tested at a high voltage range between −3.5 V and +3.5 V (Figure S4, Supporting Information). The voltage biased to the top electrode was swept from 0 to +3.5 and −3.5 V in a cycle. Two types of current−voltage plots were obtained with various reaction times. The Au/$PrGO_{DMF}$/ITO devices reacted for 20 to 60 min showed small asymmetric hysteresis loops, while the other devices (GO, $PrGO_{DMF}$ reacted for 120 min, and rGO_{N2H4}) did not exhibit current hysteresis loops. On the other hand, using Al top-electrode-deposited thin film devices (*e.g.*, Al/15 nm GO, $PrGO_{DMF}$, or rGO_{N2H4} films/ITO), the Al/$PrGO_{DMF}$/ITO devices reacted for 20−60 min showed a significant current hysteresis loop due to conductance or resistivity switching between the two states (Figure 5b and Figure S5 in Supporting Information), whereas no noticeable current hysteresis was observed in GO, $PrGO_{DMF}$ reacted for 120 min, and rGO_{N2H4}. Since the current−voltage plots showed that there were two types of memory devices with different metal top electrodes, it is believed that the electrochemical properties of each metal could be associated with memory behaviors. The electrochemically inactive gold electrode cannot be oxidized while the aluminum electrode can be electrochemically oxidized under applied positive voltages. Thus, accumulated electrons near the ITO electrode could be partially consumed to reduce $PrGO_{DMF}$ in Au/$PrGO_{DMF}$/ITO devices, leading to asymmetric current hysteresis due to the irreversible reduction of $PrGO_{DMF}$.[9] However, electrochemically oxidized aluminum ions can diffuse into the interface layer between the Al and $PrGO_{DMF}$ layers of Al/$PrGO_{DMF}$/ITO devices, and can aid in charging a portion of the active layer. Furthermore, all samples from the electrically insulating GO to the fully reduced rGO_{N2H4} were not electrochemically reduced under a voltage range from −3.5 to +3.5 V.

In the current−voltage plots of Al/$PrGO_{DMF}$/ITO devices (Figure 5b), the switching voltage from low (an OFF state) to high (an ON state) conducting states was approximately >2.0 V, which did not show specific dependence on the type of $PrGO_{DMF}$ with the reaction time, indicating that current switching is not associated with the electrochemical reduction of

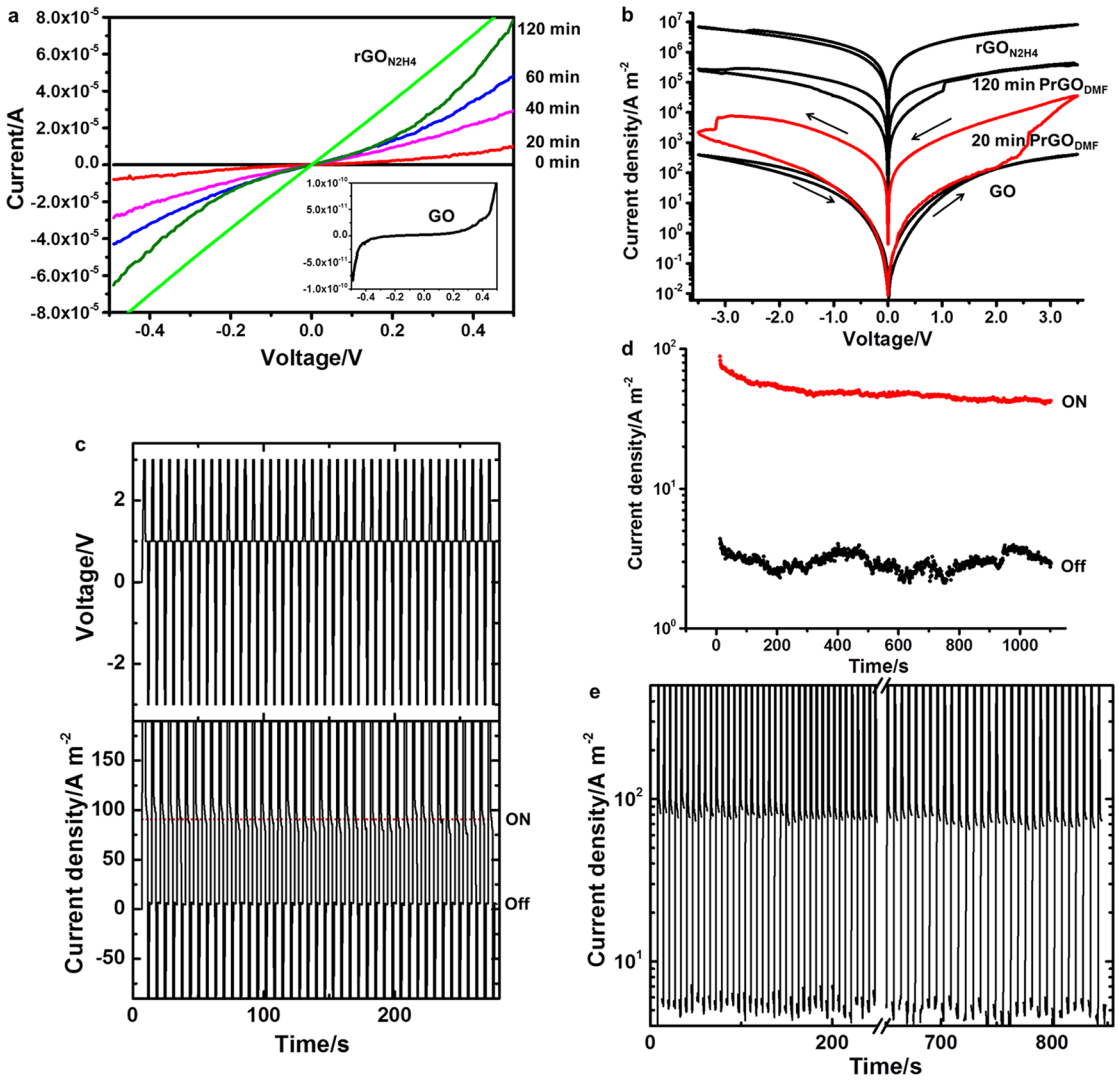

Figure 5. (a) Current−voltage plots in linear scale for GO, PrGO$_{DMF}$ and rGO$_{N2H4}$ at the low bias range from −0.5 to 0.5 V for Au(top)/GO, PrGO$_{DMF}$, rGO$_{N2H4}$/Au(bottom) devices. (b) Current−voltage plots in log scale for GO, PrGO$_{DMF}$ and rGO$_{N2H4}$ at the high bias range from 0.0 to 3.5 V and −3.5 V in a cycle for Al (top)/GO, PrGO$_{DMF}$, rGO$_{N2H4}$/ITO (bottom) devices. (c) Write-Read-Erase-Read (WRER) performance of a 20 min PrGO$_{DMF}$ device. The upper panel display applied voltage cycles for Write (3.0 V), Read (1.0 V), Erase (−3.0 V), and Read (1.0 V). The lower panel display responded current cycles in linear scale for Write, Read, Erase, and Read. (d) Current retention plots in log scale for On/Off states. (e) WRER current cycles in log scale for the device in panel c after 50 day storage.

PrGO$_{DMF}$. At 1 V, the current value of the ON state was approximately 100 times larger than that of the OFF state. The rewritable memory performances of write-read-erase-read (WRER) for the Al/PrGO$_{DMF}$/ITO devices reacted for 20 min were tested (Figure 5c). The voltages for writing, reading, and erasing were 3.0 V, 1.0 V, and −3.0 V, respectively, and the memory operation was stable for over 100 cycles of WRER. The ON/OFF ratio was approximately 100 (Figure 5c) with a retention time of >1000 s (Figure 5d). The WRER operation was preserved after 50 days of storage (Figure 5e). Thus, Figure 5c−e demonstrated crucial characteristics as a nonvolatile memory showing the stable retention and endurance performances of ON/OFF states. The PrGO$_{DMF}$ memory materials showed high stability with the short readout intervals and the long storage: (1) PrGO$_{DMF}$ as a memory material showed clear ON/OFF states and nondestructive states during much readout (1100 times) for the short time (1000 s). (2) The stable endurance performance after 50-day storage is long enough. In addition, the *I*−*V* characteristic tests of each device were performed under ambient condition as well as vacuum, and no effects of oxygen or water were not found. Intercalated water molecules (for GO) or oxygen groups (for PrGO$_{DMF}$) in each film could not destruct the device performance during a long storage.

According to the literature, partially reduced GO exhibits stable memory behavior in comparison with nonreduced GO, indicating that some degree of oxygen content influences GO-based memory effects.[9] In this study, only semiconducting PrGO$_{DMF}$ with an

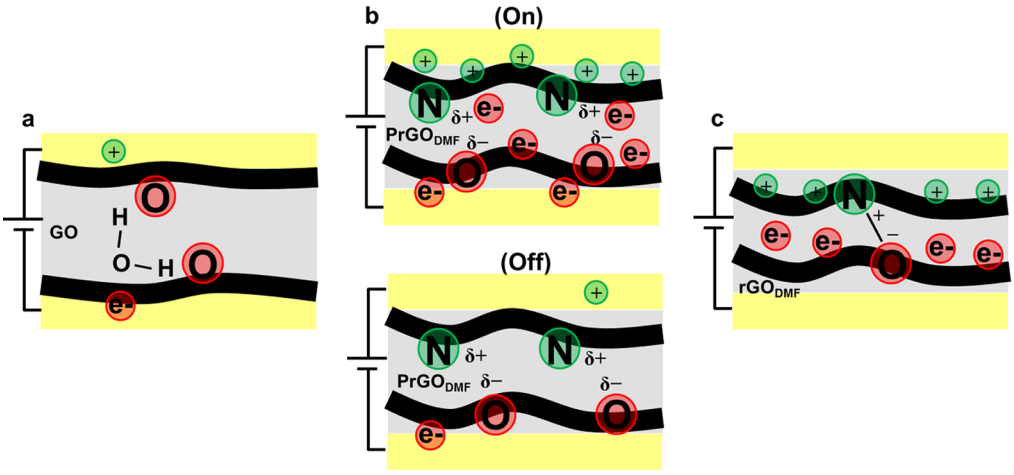

Figure 6. Schematic of the proposed switching mechanism of two conducting states for an N-doped PrGO$_{DMF}$ memory device; (a) Al/GO/ITO, (b) Al/PrGO$_{DMF}$/ITO, (c) Al/rGO$_{DMF}$/ITO.

oxygen-functionalized carbon density of 45−50% induced the bistable resistivity associated with rewritable nonvolatile memory. Moreover, insulating GO, decarboxylated PrGO$_{DMF}$ (*i.e.*, defunctionalization of carboxylic groups), and highly conducting rGO$_{N2H4}$ devices did not exhibit current hysteresis loops, indicating that the factors determining the memory behavior of PrGO$_{DMF}$ included not only the oxygen content (or the oxygen-functionalized carbon density) of GO (or rGO), but also the formation of $H^{\delta+}$N-PrGO−$COO^{\delta-}$/$H^{\delta+}$N-PrGO−$COO^{\delta-}$ in the interlayers. Therefore, our results revealed that, in addition to the oxygen content or the oxygen-functionalized carbon density, the interplay of functional groups between PrGO sheets is an important factor to determine the memory characteristics.

Figure 6 shows a schematic of the proposed switching mechanism of the two conducting states for an N-doped PrGO$_{DMF}$ memory device. (1) The pristine GO device has many water molecules intercalated in a relatively thick interlayer, which serves as an insulating barrier between the GO framework and the oxygen functional groups. On the other hand, (2) N-doped PrGO$_{DMF}$, particularly pyridinium N, has a relatively small insulating barrier due to the insertion of nitrogen atoms and the reduction of the intercalated water molecules and oxygen functional groups. In addition, a charge transport path could be formed through the association between pyridinium N doped PrGO$_{DMF}$ frameworks and charged oxygen functional groups, switching an OFF state to an ON state as a result of the voltage-induced polarization of the film. However, (3) when oxygen functional groups such as carboxyl groups are removed, the polarization effect becomes weak and the resulting charge transport path no longer forms, resulting in no observable current hysteresis loops for 120 min PrGO$_{DMF}$ and rGO$_{N2H2}$ devices.

CONCLUSIONS

In conclusion, chemically synthesized N-doped semiconducting PrGOs were produced using a mild reducing agent, the polar aprotic solvent DMF, and yielded different band gap values. Reaction time-dependent GO reduction with DMF resulted in a variety of optical band gaps from 2.55 eV (GO) to 1.35 eV (120 min PrGO$_{DMF}$). In two-terminal memory devices with the N-doped semiconducting PrGOs sandwiched between top and bottom metal electrodes, the current hysteresis exhibited two conducting states in current−voltage characteristics. However, for fully reduced GO with a low oxygen-functionalized carbon density (small amount of a negatively charged oxygen) and highly oxidized GO with a high oxygen-functionalized carbon density (no positively charged pyridinium), the current hysteresis was negligible. As carefully designed, the semiconducting PrGO$_{DMF}$ devices containing sp^2 C=C frameworks with 2.7−3.2% nitrogen atoms and an oxygen-functionalized carbon density of 45−50% (especially ∼1.5% pyridinium N atoms) clearly displayed rewritable nonvolatile memory behaviors, suggesting that novel N-doped PrGO$_{DMF}$ could form a charge transporting path by associating with oxygen/nitrogen-functional groups such as $H^{\delta+}$N-PrGO−$COO^{\delta-}$/$H^{\delta+}$N-PrGO−$COO^{\delta-}$ in interlayers of PrGO$_{DMF}$ sheets. As a whole, the voltage-induced polarization of the film allowed the switching of an OFF state to an ON state, producing a rewritable nonvolatile memory.

METHODS

Sample Preparation. GO was synthesized using a modified Hummers method from graphite powders (Bay Carbon, SP-2) and purified according to previous reports.[26−28] GO sheets (approximately 1.0 mg mL^{-1}) were dissolved in solvent (DI water) or a solvent mixture (DMF:DI H_2O, 9:1) followed by ultrasonication. The GO solution was thermally reduced under

reflux conditions in an oil bath (or an autoclave) at 150 °C under an Ar gas (10% H_2) atmosphere. A cooling condenser was used to prevent solvent evaporation. The product was filtered or directly drop-casted on chemically cleaned substrates, predried at room temperature in the air, and dried at 80 °C for 24 h in a vacuum oven.

Thermal Annealing. Dried samples of both GO and chemically reduced rGO_{N2H4} (with hydrazine) in a vacuum oven at 80 °C for 24 h were thermally reduced or annealed by a programmed heating/cooling process under Ar containing 10% H_2 by a rapid thermal annealing (RTA) system (SAM Vac CS410, Eurotherm 2040 Temperature controller). The samples were initiated at room temperature, rapidly heated to high temperature within a few tens of seconds (30 or 90 s), and then slowly cooled to room temperature within 15 min.

Characterization. Raman spectroscopy was performed at 514 nm on samples on SiO_2 substrates. FT-IR spectroscopy (Bruker IFS-66/S) and X-ray diffraction (Ultima IV, Rigaku) were performed using highly pressurized pellets of ground powder samples. X-ray photoelectron spectroscopy (VG Microtech ESCA 2000) and UV−vis diffuse reflectance spectroscopy (UV-3600, Shimadzu) were performed using drop-cast samples on Si substrates.

Fabrication and Measurement of Memory Devices. The synthesized solutions were spin-coated to produce a thin film (~15 nm) on a precleaned ITO (or Au) electrode. The samples were dried in a vacuum oven at 80 °C for 24 h. Au top electrodes (60 nm thick) or Al top electrodes (80 nm thick) were deposited by electron-beam evaporation at a low deposition rate (0.1 Å s^{-1}). The electrical characteristics of the memory devices were measured (a Keithley 4200−SCS semiconductor characterization system) in a vacuum (approximately $1.0 \times 10^{-4} \sim 1.0 \times 10^{-5}$ Torr).

Conflict of Interest: The authors declare no competing financial interest.

Acknowledgment. This work was supported by the Creative Research Initiatives (project title: Smart Molecular Memory) of MOST/KOSEF.

Supporting Information Available: (1) Table for XPS data, (2) XPS spectra, (3) UV−vis diffuse reflectance spectra, (4) XRD spectra, and (5) current−voltage plots. This material is available free of charge *via* the Internet at http://pubs.acs.org.

REFERENCES AND NOTES

1. Heremans, P.; Gelinck, G. H.; Müller, R.; Baeg, K. J.; Kim, D. Y.; Noh, Y. Y. Polymer and Organic Nonvolatile Memory Devices. *Chem. Mater.* **2011**, *23*, 341–358.
2. Dimitrakopoulos, C. D.; Malenfant, P. R. L. Organic Thin Film Transistors for Large Area Electronics. *Adv. Mater.* **2002**, *14*, 99–117.
3. Tseng, C. W.; Tao, Y. T. Electric Bistability in Pentacene Film-Based Transistor Embedding Gold Nanoparticles. *J. Am. Chem. Soc.* **2009**, *131*, 12441–12450.
4. Hahm, S. G.; Kang, N. G.; Kwon, W.; Kim, K.; Ko, Y. G.; Ahn, S.; Kang, B. G.; Chang, T.; Lee, J. S.; Ree, M. Programmable Bipolar and Unipolar Nonvolatile Memory Devices Based on Poly(2-(N-carbazolyl)ethyl methacrylate) End-Capped with Fullerene. *Adv. Mater.* **2012**, *24*, 1062–1066.
5. Hwang, S. K.; Lee, J. M.; Kim, S.; Park, J. S.; Park, H. I.; Ahn, C. W.; Lee, K. J.; Lee, T.; Kim, S. O. Flexible Multilevel Resistive Memory with Controlled Charge Trap B- and N-doped Carbon Nanotubes. *Nano Lett.* **2012**, *12*, 2217–2221.
6. He, C. L.; Zhuge, F.; Zhou, X. F.; Li, M.; Zhou, G. C.; Liu, Y. W.; Wang, J. Z.; Chen, B.; Su, W. J.; Liu, Z. P.; Wu, Y. H.; Cui, P.; Li, R. W. Nonvolatile Rsistive Switching in Graphene Oxide Thin Films. *Appl. Phys. Lett.* **2009**, *95*, 232101.
7. Yu, W. J.; Chae, S. H.; Lee, S. Y.; Duong, D. L.; Lee, Y. H. Ultra-Transparent, Flexible Single-Walled Carbon Nanotube Non-Volatile Memory Device with An Oxygen-Decorated Graphene Electrode. *Adv. Mater.* **2011**, *23*, 1889–1893.
8. Jeong, H. Y.; Kim, J. Y.; Kim, J. W.; Hwang, J. O.; Kim, J. E.; Lee, J. Y.; Yoon, T. H.; Cho, B. J.; Kim, S. O.; Ruoff, R. S.; Choi, S. Y. Graphene Oxide Thin Films for Flexible Nonvolatile Memory Applications. *Nano Lett.* **2010**, *10*, 4381–4386.
9. Zhao, F.; Liu, J.; Huang, X.; Zou, X.; Lu, G.; Sun, P.; Wu, S.; Ai, W.; Yi, M.; Qi, X.; Xie, L.; Wang, J.; Zhang, H.; Huang, W. Chemoselective Photodeoxidization of Graphene Oxide Using Sterically Hindered Amines as Catalyst: Synthesis and Applications. *ACS Nano* **2012**, *6*, 3027–3033.
10. Liu, J.; Yin, Z.; Cao, X.; Zhao, F.; Wang, L.; Huang, W.; Zhang, H. Fabrication of Flexible, All-Reduced Graphene Oxide Non-Volatile Memory Devices. *Adv. Mater.* **2013**, *25*, 233–238.
11. He, C. L.; Zhuge, F.; Zhou, X. F.; Li, M.; Zhou, G. C.; Liu, Y. W.; Wang, J. Z.; Chen, B.; Su, W. J.; Liu, Z. P.; Wu, Y. H.; Cui, P.; Li, R. W. Nonvolatile Resistive Switching in Graphene Oxide Thin Films. *Appl. Phys. Lett.* **2009**, *95*, 232101.
12. Chang, H.; Sun, Z.; Yuan, Q.; Ding, F.; Tao, X.; Yan, F.; Zheng, Z. Thin Film Field-Effect Phototransistors from Bandgap-Tunable, Solution-Processed, Few-Layer Reduced Graphene Oxide Films. *Adv. Mater.* **2010**, *22*, 4872–4876.
13. Dreyer, D. R.; Park, S.; Bielawski, C. W.; Ruoff, R. S. The Chemistry of Graphene Oxide. *Chem. Soc. Rev.* **2010**, *39*, 228–240.
14. Park, S.; An, J.; Jung, I.; Piner, R. D.; An, S. J.; Li, X.; Velamakanni, A.; Ruoff, R. S. Colloidal Suspensions of Highly Reduced Graphene Oxide in A Wide Variety of Organic Solvents. *Nano Lett.* **2009**, *9*, 1593–1597.
15. Carpenter, M. K.; Moylan, T. E.; Kukreja, R. S.; Atwan, M. H.; Tessema, M. M. Solvothermal Synthesis of Platinum Alloy Nanoparticles for Oxygen Reduction Electrocatalysis. *J. Am. Chem. Soc.* **2012**, *134*, 8535–8542.
16. Sheng, Z.-H.; Shao, L.; Chen, J.-J.; Bao, W.-J.; Wang, F.-B.; Xia, X.-H. Catalyst-Free Synthesis of Nitrogen-Doped Graphene *via* Thermal Annealing Graphite Oxide with Melamine and Its Excellent Electrocatalysis. *ACS Nano* **2011**, *5*, 4350–4358.
17. Yang, D.; Velamakanni, A.; Bozoklu, G.; Park, S.; Stoller, M.; Piner, R. D.; Stankovich, S.; Jung, I.; Field, D. A.; Ventrice, C. A., Jr; Ruoff, R. S. Chemical Analysis of Graphene Oxide Films After Heat and Chemical Treatments by X-Ray Photoelectron and Micro-Raman Spectroscopy. *Carbon* **2009**, *47*, 145–152.
18. Krishnan, S.; Ward, R. J.; Hexemer, A.; Sohn, K. E.; Lee, K. L.; Angert, E. R.; Fischer, D. A.; Kramer, E. J.; Ober, C. K. Surfaces of Fluorinated Pyridinium Block Copolymers with Enhanced Antibacterial Activity. *Langmuir* **2006**, *22*, 11255–11266.
19. Fukuda, N.; Ishida, N.; Nomura, K.; Wang, T.; Tamada, K.; Ushijima, H. Analysis of Adsorption and Binding Behaviors of Silver Nanoparticles onto A Pyridyl-Terminated Surface Using XPS and AFM. *Langmuir* **2011**, *27*, 12916–12922.
20. Wang, H.; Maiyalagan, T.; Wang, X. Review on Recent Progress in Nitrogen-Doped Graphene: Synthesis, Characterization, and Its Potential Applications. *ACS Catal.* **2012**, *2*, 781–794.
21. Yoon, Y.; Seo, S.; Kim, G.; Lee, H. Atomic Dopants Involved in The Structural Evolution of Thermally Graphitized Graphene. *Chem.—Eur. J.* **2012**, *18*, 13466–13472.
22. Misra, A.; Tyagi, P. K.; Singh, M. K.; Misra, D. S. FTIR Studies of Nitrogen Doped Carbon Nanotubes. *Diamond Relat. Mater.* **2006**, *15*, 385–388.
23. Jeong, H. K.; Jin, M. H.; So, K. P.; Lim, S. C.; Lee, Y. H. Tailoring the Characteristics of Graphite Oxides by Different Oxidation Times. *J. Phys. D: Appl. Phys.* **2009**, *42*, 065418.
24. López, R.; Gómez, R. Band-Gap Energy Estimation from Diffuse Reflectance Measurements on Sol-Gel and Commercial TiO_2: A Comparative Study. *J. Sol-Gel Sci. Technol.* **2012**, *61*, 1–7.
25. Huh, S. H., Thermal Reduction of Graphene Oxide. In *Physics and Applocations of Graphene—Experiments*; Mikhailov, D. S., Ed.; InTech: New York, 2011.
26. Tung, V. C.; Allen, M. J.; Yang, Y.; Kaner, R. B. High-Throughput Solution Processing of Large-Scale Graphene. *Nat. Nanotechnol.* **2009**, *4*, 25–29.
27. Wang, X.; Zhi, L.; Müllen, K. Transparent, Conductive Graphene Electrodes for Dye-sensitized Solar Cells. *Nano Lett.* **2008**, *8*, 323–327.
28. Moon, I. K.; Lee, J.; Ruoff, R. S.; Lee, H. Reduced Graphene Oxide by Chemical Graphitization. *Nat. Commun.* **2010**, *1*, 73.